Journal of Materials Chemistry A

Accepted Manuscript

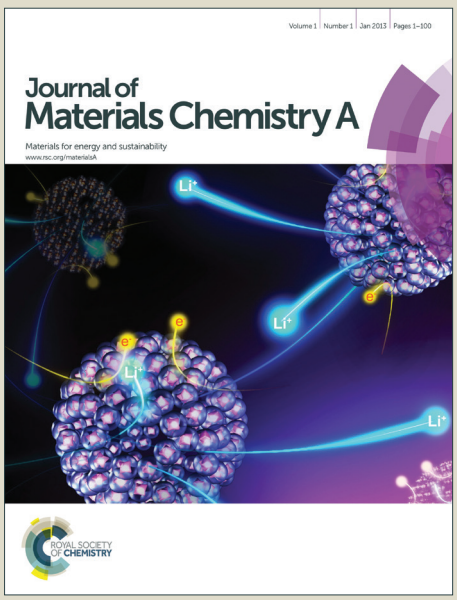

ROYAL SOCIETY OF CHEMISTRY

www.rsc.org/materialsA

Journal Name

RSCPublishing

ARTICLE

Influence of moiety sequence on the performance of small molecular photovoltaic materials

Cite this: DOI: 10.1039/x0xx00000x

Received 00th January 2012,
Accepted 00th January 2012

DOI: 10.1039/x0xx00000x

www.rsc.org/

Long Liang,[a] Jin-Tu Wang,[a] Xuan Xiang,[b] Jun Ling,[c] Fu-Gang Zhao[b] and Wei-Shi Li*[ab]

The purpose of this work is to study the impact of moiety sequence in chemical structure of small molecular photovoltaic materials on their basic properties and photovoltaic performance. For this aim, two isomeric compounds, namely **BDT(ThBTTh)$_2$** and **BDT(BTTh$_2$)$_2$**, with a structural variation by exchanging benzothiadiazole and thiophene positions, have been designed and synthesized. As compared with **BDT(BTTh$_2$)$_2$**, **BDT(ThBTTh)$_2$** possesses a lower melting point, a blue-shifted absorption spectrum in solution, and slightly lower-lying highest occupied and lowest unoccupied molecular orbitals. More interestingly, the hole mobility of **BDT(ThBTTh)$_2$** neat film is 0.1 $cm^2 V^{-1} s^{-1}$, three-order larger than that of **BDT(BTTh$_2$)$_2$**. Furthermore, these two compounds display much different photovoltaic performance, 4.53% for **BDT(ThBTTh)$_2$** versus 1.58% for **BDT(BTTh$_2$)$_2$** in term of power conversion efficiency.

Introduction

Organic solar cells (OSCs) have attracted great attention for their advantages of low cost, flexibility, light weight and easy fabrication.[1] Conjugated polymers, especially donor–acceptor (D–A) type, are one of the promising donor materials for bulk heterojunction (BHJ) OSCs.[1, 2] With the rapid development of high performance D–A conjugated polymers recently, the power conversion efficiency (PCE) of a single module OSC device has exceeded 8%,[3] while that of a tandem model over 10%.[4] However, since polymers are the mixtures of homologues, they always have issues of average molecular weight and its polydispersity. It has been demonstrated that molecular weight has great impact on the photovoltaic properties of conjugated polymers. Therefore, conjugated polymer photovoltaic materials generally suffer from property variations batch-by-batch. Besides conjugated polymers, small molecular compounds with effective light harvesting in visible and near infrared region have also been applied as donor materials for BHJ OSCs.[5] Comparing to polymers, small molecular materials can avoid batch-dependent problems owing to their definite chemical structures and high purity achievable by many purification techniques. Up to date, a variety of solution-processable small molecules with different structures including linear, star-like, and hyperbranched type have been reported.[5] However, only a few works showed comparable photovoltaic performance to conjugated polymers.[6–8] These included a series of molecular photovoltaic compounds, developed by Chen and his coworkers.[6] A PCE up to 8.12% has been achieved with a compound using thienyl benzodithiophene (BDT) as a core and 3-ethylrhodanine as terminal group.[6c] Bazan, Heeger, *et al.* reported DTS(PTTh$_2$)$_2$[7] and DTS(FBTTh$_2$)$_2$[8] using dithienosilole (DTS) as donor core while [1,2,5]-thiadiazolo-[3,4-*c*]-pyridine or fluorobenzo-thiadiazole as arms, both showing promising photovoltaic performance with a PCE up to 9.02%.[8b] Although there are plenty of studies aiming to disclose the structure-property relationships for molecular photovoltaic materials,[5] it is still difficult to answer how to design a compound that would gain high performance. We noticed that the most works were endeavoured to investigate the impact of different optoelectronic moieties and their combination, as well as side chain engineering. Less attention was paid on the influence of moiety sequence. In this work, we report two isomeric compounds named **BDT(ThBTTh)$_2$** and **BDT(BTTh$_2$)$_2$** (Fig. 1). They are composed of one benzodithiophene (BDT), two benzothiadiazole (BT) and four thiophene (Th) units, but have different moiety sequence. Of interest, these two compounds

exhibited totally different photovoltaic performance. A PCE of 4.5% was achieved for **BDT(ThBTTh)$_2$**-based OSC devices, while those based on **BDT(BTTh$_2$)$_2$** only displayed a best PCE as low as 1.6%.

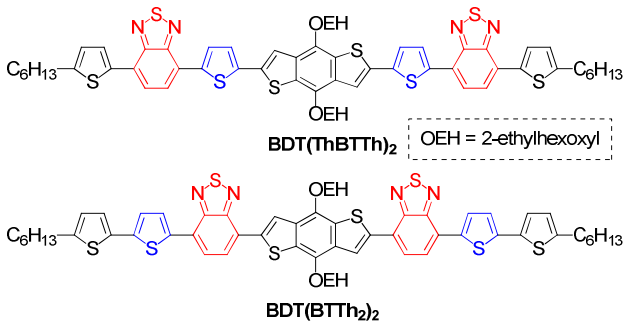

Fig. 1 Molecule structures of **BDT(ThBTTh)$_2$** and **BDT(BTTh$_2$)$_2$**.

Results and discussion

Synthesis and thermal properties

The syntheses of **BDT(ThBTTh)$_2$** and **BDT(BTTh$_2$)$_2$** are outlined in Scheme 1. One of the key steps for both compounds is mono Suzuki coupling of 4,7-dibromobenzo[*c*][1,2,5]thiadiazole. For this reaction, an excess amount of 4,7-dibromobenzo[*c*][1,2,5]thiadiazole was used and afforded compound **3** in a yield of 70%, while 48% for compound **5**. Stille coupling was applied for the final step for both **BDT(ThBTTh)$_2$** and **BDT(BTTh$_2$)$_2$**. The molar ratio between the brominated starting material (compound **3** or **5**) and 4,8-bis(2-ethylhexoxyl)benzo[1,2-*b*:4,5-*b*']dithiophene-2,6-diyl) bistrimethylstannane was 2.5 : 1. **BDT(ThBTTh)$_2$** was obtained in a yield of 58%, while 91% for **BDT(BTTh$_2$)$_2$**. Due to their large rigid rod-like structures and small side chains, these two compounds did not display good solubility at room temperature, only limitedly dissolvable in chloroform, chlorobenzene, toluene, and so on. However, their solubility could be raised over 15 mg mL^{-1} in slightly heated solutions, which ensures the processing feasibility for both compounds.

Thermogravimetric analysis (TGA) revealed good thermal stabilities for both compounds, with a 5%-weight loss temperature (Td) of 335.2 °C for **BDT(ThBTTh)$_2$**, while 340.4 °C for **BDT(BTTh$_2$)$_2$** (Fig. S1, ESI†). In the differential scanning calorimetry (DSC) profile, **BDT(ThBTTh)$_2$** displayed a sharp endothermic peak at 202.5 °C and a sharp exothermic peak at 192.8 °C in the second heating-cooling cycle (Fig. S2, ESI†). These peaks are attributed to melting and crystallizing phase transition, respectively, confirmed by polarized optical microscopy. In addition to these peaks, a pair of broad thermal transitions around 145 °C were also observed in the DSC profile of **BDT(ThBTTh)$_2$**. These may originate from certain solid-to-solid transition. In comparison, **BDT(BTTh$_2$)$_2$** exhibited melting and crystallizing phase transition at 213.8 and 204.4 °C, both higher than those of **BDT(ThBTTh)$_2$**. This fact suggests that the isomer **BDT(BTTh$_2$)$_2$** has stronger intermolecular interactions than **BDT(ThBTTh)$_2$**.

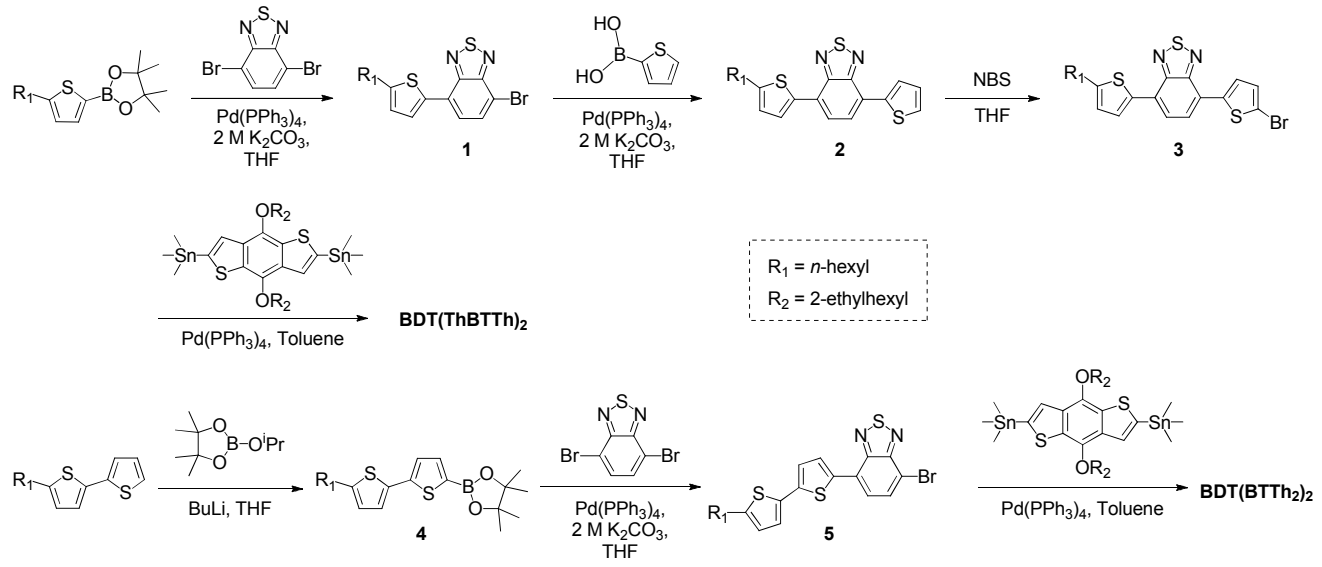

Scheme 1 Syntheses of **BDT(ThBTTh)$_2$** and **BDT(BTTh$_2$)$_2$**.

Optical and electrochemical properties

Fig. 2a displays the absorption spectra of these two compounds in chlorobenzene with a concentration of 1 × 10^{-5} M, while their absorption peaks and molar extinction coefficients are summarized in Table 1. It is clearly that **BDT(BTTh$_2$)$_2$** showed two main absorption bands centred at 368 and 569 nm. The latter is assignable to the absorption band originating from the intramolecular charge transfer (ICT) between electron-deficient BT units and electron-rich BDT and thiophene units, while the former may come from local π-π* transition of the conjugated core. In comparison, the ICT absorption band of

BDT(ThBTTh)$_2$ appeared at 526 nm, 43 nm blue-shifted to that of **BDT(BTTh$_2$)$_2$**. The molar extinction coefficient of this band was estimated to be 6.5 × 10^4 M^{-1} cm^{-1}, slightly larger than that for **BDT(BTTh$_2$)$_2$** (5.5 × 10^4 M^{-1} cm^{-1}). Besides the ICT band, the absorption spectrum of **BDT(ThBTTh)$_2$** displayed two additional peaks at 314 and 398 nm in the range of 300–650 nm. The nature of the latter would be the same as the peak at 368 nm in **BDT(BTTh$_2$)$_2$** spectrum, although their maximum wavelengths have a difference of 30 nm. Obviously, all the above spectral differences in solution are due to the structural variation between **BDT(ThBTTh)$_2$** and **BDT(BTTh$_2$)$_2$**, in which BT and one thiophene units exchange their positions.

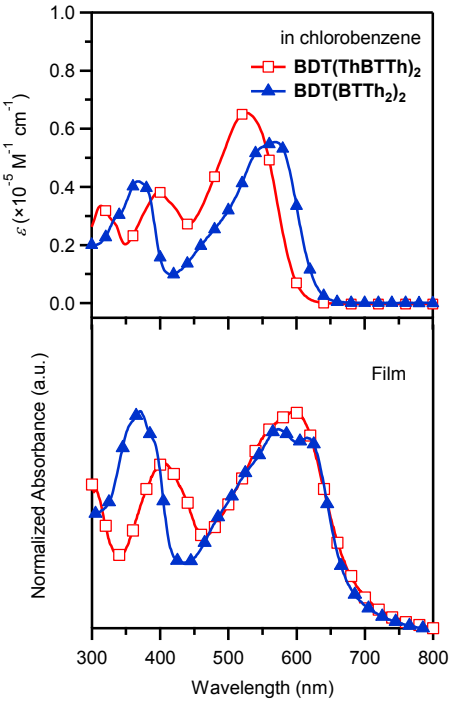

Fig. 2 UV-vis absorption spectra of **BDT(ThBTTh)$_2$** and **BDT(BTTh$_2$)$_2$** in chlorobenzene solutions and in film state measured at room temperature.

Table 1 Optical and electrochemical properties of **BDT(ThBTTh)$_2$** and **BDT(BTTh$_2$)$_2$**.

Compound	λ_{max} (nm)		$E_{ox,\ onset}$ (V)	HOMO (eV)	LUMO (eV)	$E_{g,\ opt}$ (eV)
	Solution [a]	Film				
BDT(ThBTTh)$_2$	314 (3.3) 398 (3.8) 526 (6.5)	406 596	0.52	–5.17	–3.40	1.77
BDT(BTTh$_2$)$_2$	368 (4.2) 569 (5.5)	372 573 615	0.46	–5.11	–3.34	1.77

[a] Data in parentheses are molar extinct coefficients in a unit of 10^4 M^{-1} cm^{-1}.

In film state, the ICT band of **BDT(ThBTTh)$_2$** appeared at 596 nm, 70 nm red-shifted from that in chlorobenzene solution (Fig. 2b). However, in the case of **BDT(BTTh$_2$)$_2$** film, there were two apexes at 573 and 615 nm for this band, which were 4 and 46 nm respectively red-shifted from its ICT peak in solution. Although they had different apexes, it should be noticed that these film ICT bands of both compounds covered the completely same spectral region and had a superimposed shape except the apexes. The onset absorption sites for the both films were estimated to be 700 nm, giving a optical energy gap ($E_{g,\ opt}$) of 1.77 eV for both **BDT(ThBTTh)$_2$** and **BDT(BTTh$_2$)$_2$**.

The electrochemical properties of **BDT(ThBTTh)$_2$** and **BDT(BTTh$_2$)$_2$** were investigated by cyclic voltammetry (CV, Fig. S3, ESI†) with film samples casting from their chlorobenzene solutions onto glassy carbon electrodes. The onset oxidation potentials (E_{ox}) *vs.* Ag/Ag^+ were measured to be 0.52 V for **BDT(ThBTTh)$_2$** and 0.46 V for **BDT(BTTh$_2$)$_2$** (Table 1). Ferrocene/ferrocenium (Fc/Fc^+), which has a standard energy level of –4.8 eV from vacuum,[9] was used as an internal reference and determined to be 0.15 V *vs.* Ag/Ag^+ under the same conditions. Therefore, the highest occupied molecular orbital (HOMO) energy level can be calculated by the equation of HOMO = − e (E_{ox} + 4.65), giving –5.17 eV for **BDT(ThBTTh)$_2$** and –5.11 eV for **BDT(BTTh$_2$)$_2$**. The former is slightly lower than the latter, which may be good for its photovoltaic performance. Calculated from HOMO and $E_{g,opt}$, the lowest unoccupied molecular orbital (LUMO) energy levels were estimated to be –3.40 eV for **BDT(ThBTTh)$_2$** and –3.34 eV for **BDT(BTTh$_2$)$_2$**.

Theoretical study

To gain insight into the fundamental structural and electronic properties of **BDT(ThBTTh)$_2$** and **BDT(BTTh$_2$)$_2$**, density functional theory (DFT) study was performed at B3LYP/6-311+G**//B3LYP/6-31G* level[10] using a GAUSSIAN03 program package.[11] To simplify the calculation, methyl group was used to replace all alkyl side chains in the model compounds. The optimized molecular geometries are displayed in Fig. 3. It is clear that the exchange of BT and thiophene units affords different molecular geometries. Compound **BDT(BTTh$_2$)$_2$** possesses a long and straightforward linear central part, which is composed of one BDT and two BT units. The directions of two thienyl units in both ends begin to deviate from the central line of the molecule. In contrast, the insertion of a thienyl unit between BT and BDT in **BDT(ThBTTh)$_2$** results in a more zigzag-like molecular shape. Although both compounds exhibit a good planar structure for π-conjugation, there are subtle differences in dihedral angles among the moieties. For **BDT(ThBTTh)$_2$**, three dihedral angles from central BDT to the end thienyl unit are 1.6, 1.4, and 0.2 °. Whereas, these angles are 3.6, 1.5, and 10.0 ° for **BDT(BTTh$_2$)$_2$**, larger than those of **BDT(ThBTTh)$_2$**. The different molecular geometry and shape may affect the molecular packing structure in solid state, and then influence their properties.

Fig. 3 also shows the electron wave functions of the HOMO and LUMO orbitals. For HOMO, electron obviously delocalizes throughout the whole molecular structure, suggesting a good π-electron conjugation for both compounds. However for LUMO, electron density is mainly residing on BT units, confirming these two compounds are typical D–A type.

Besides BT units, electron density of LUMO is partially distributed on central BDT unit for **BDT(BTTh$_2$)$_2$**. While in the case of **BDT(ThBTTh)$_2$**, partial electron density of LUMO is on thienyl units, not central BDT. This subtle difference may influence the LUMO energy level of the compound. Therefore, the calculated LUMO energy level is –3.078 eV for **BDT(ThBTTh)$_2$**, a little higher from that for **BDT(BTTh$_2$)$_2$** (–3.144 eV). With the calculated HOMO energy level (**BDT(ThBTTh)$_2$**: –5.169 eV, **BDT(BTTh$_2$)$_2$**: –5.171 eV), the theoretical energy gap is 2.03 eV for **BDT(ThBTTh)$_2$**, while 2.09 eV for **BDT(BTTh$_2$)$_2$**.

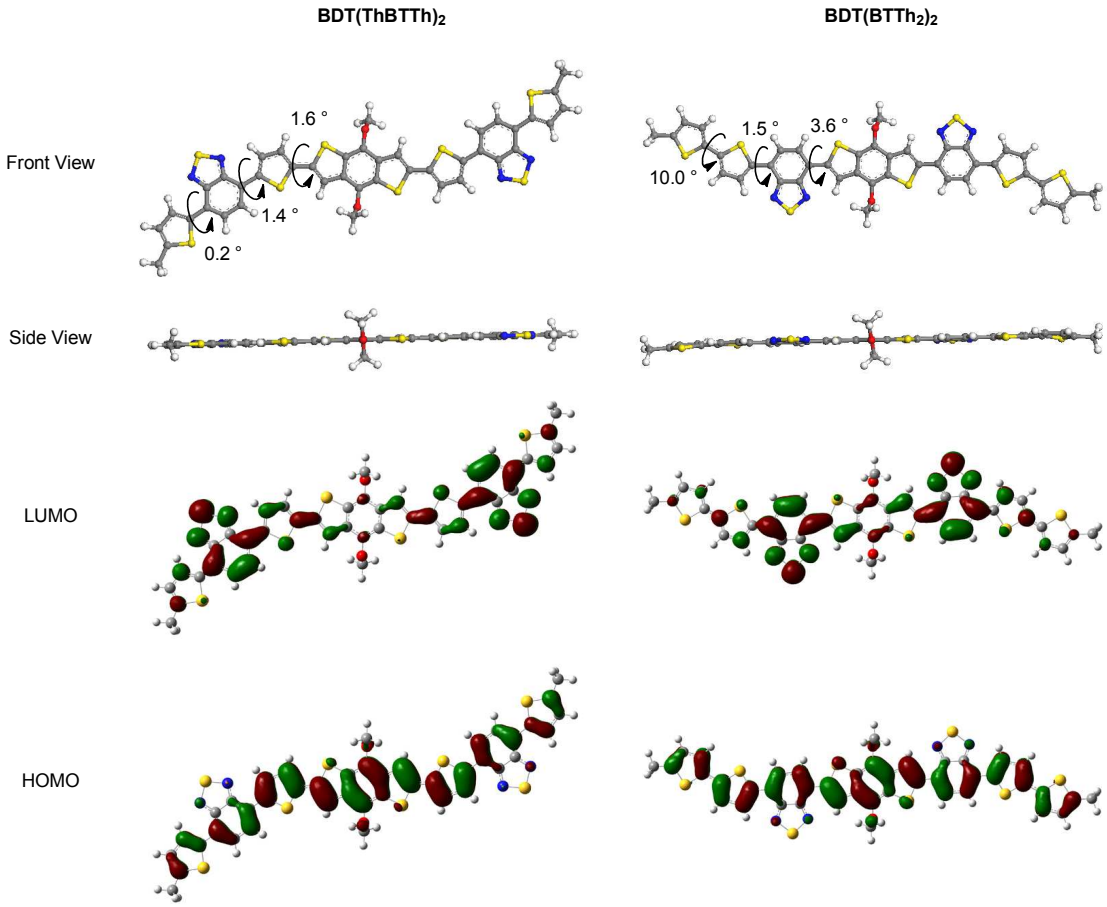

Fig. 3 DFT computed molecular geometries and electron wave functions of HOMO and LUMO orbitals for **BDT(ThBTTh)$_2$** and **BDT(BTTh$_2$)$_2$**.

Photovoltaic performance

The photovoltaic performance of **BDT(ThBTTh)$_2$** and **BDT(BTTh$_2$)$_2$** was investigated using bulk heterojunction devices with a structural configuration of ITO/PEDOT:PSS/active layer/Ca/Al. The active layer was fabricated by spin-coating a chlorobenzene solution containing a mixture of checked compound (**BDT(ThBTTh)$_2$** or **BDT(BTTh$_2$)$_2$**) and [6,6]-phenyl-C_{61}-butyric acid methyl ester ($PC_{61}BM$). For both **BDT(ThBTTh)$_2$** and **BDT(BTTh$_2$)$_2$** devices, the weight ratio of the checked compound to $PC_{61}BM$, the concentration of the processing solution, and annealing temperature were optimized and found to be 1/1, 30 mg L^{-1} and 120 °C, respectively. The current density–voltage curves of their best devices are displayed in Fig. 4a, while the corresponding device parameters are summarized in Table 2. Of interest, the optimized **BDT(ThBTTh)$_2$**-based device displayed a much better performance than that based on **BDT(BTTh$_2$)$_2$**. The former device showed an open-circuit voltage (V_{OC}) of 0.89 V, a short-circuit current (J_{SC}) of 9.33 mA cm^{-2}, and a fill factor (FF) of 54.5%, giving a PCE of 4.53%. Whereas for the latter, these parameters changed to 0.82 V, 4.74 mA cm^{-2} and 40.5%, respectively, giving a PCE of 1.58%. Considering the fact that **BDT(ThBTTh)$_2$** and **BDT(BTTh$_2$)$_2$** are isomers with a structural variation only in the sequence of BT and thiophene units, the observed so large difference in photovoltaic performance is amazing.

Obviously, the performance improvement for **BDT(ThBTTh)$_2$** cell as referred to that based on **BDT(BTTh$_2$)$_2$** mainly came from the enhancement in J_{SC} and FF parameters. For J_{SC}, the enhancement reached as high as 97%. To further understand this improvement, the external quantum efficiency (EQE) spectroscopy was performed on the above two optimized cells. As shown in Fig. 4b, the EQE spectra reveal a completely same photo-response spectral range from 300 to 700 nm for both cells. This is well consistent with

the observation in the film absorption spectroscopy, in which **BDT(ThBTTh)$_2$** and **BDT(BTTh$_2$)$_2$** displayed the same spectral coverage. However, EQE values in the range of 350–600 nm were 50–60% for **BDT(ThBTTh)$_2$** cell, much larger than those for **BDT(BTTh$_2$)$_2$** cell (mostly in 15–30%).

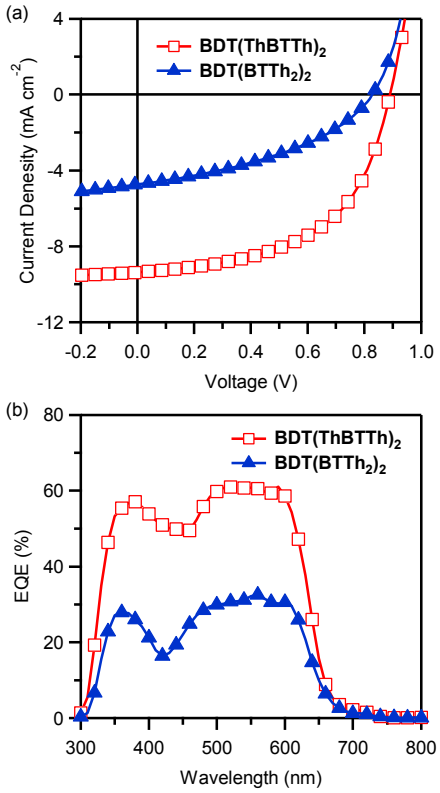

Fig. 4 (a) Current density-voltage curves under the illumination of AM 1.5 G with a density of 100 mW cm^{-2} and (b) EQE spectra of the optimized OSC devices based on **BDT(ThBTTh)$_2$** and **BDT(BTTh$_2$)$_2$** with $PC_{61}BM$.

Table 2 Device parameters of the OSC devices shown in Fig. 4a and hole mobility for **BDT(ThBTTh)$_2$**- or **BDT(BTTh$_2$)$_2$**-based neat films and blend films with $PC_{61}BM$ (1:1, w/w)

Compound	V_{OC} (V)	J_{SC} [a] (mA cm^{-2})	FF (%)	PCE [b] (%)	μ_h (10^{-4} cm^2 V^{-1} s^{-1})	
					Neat[c]	Blend[d]
BDT(ThBTTh)$_2$	0.89	9.33 (9.02)	54.5	4.53 (4.45)	1000	4.7 (110 nm) 2.2 (95 nm)
BDT(BTTh$_2$)$_2$	0.82	4.74 (4.53)	40.5	1.58 (1.50)	2.4	0.69 (100 nm) 0.86 (70 nm)

[a] Data in parentheses are calculated from EQE spectra shown in Fig. 4b; [b] Data in parentheses are the average values; [c] measured by OFET method; [d] measured by SCLC method. Data in parentheses are the thicknesses of the blend films.

Hole mobility, film structure and morphology

In order to know the origination of the observed photovoltaic performance differences between **BDT(ThBTTh)$_2$** and **BDT(BTTh$_2$)$_2$**, we carried out more detailed investigations on their charge mobility, structure and morphology of their neat and blend films with $PC_{61}BM$. Charge mobility is one of the main factors that determines the material photovoltaic performance, mainly in J_{SC} and FF parameters.[12] The hole mobilities of these two compounds in neat film were measured by means of organic field-effect transistor (OFET) devices with a structure configuration of bottom gate top contact. The devices were fabricated on octadecyltrichlorosilane (OTS)-modified Si/SiO_2 plates and using Au as source and drive electrodes. Both these two compounds displayed typical *p*-channel charge transportation characteristics (Fig. S5, ESI†). Estimated from the saturated regime, the hole mobility was estimated to be 0.1 cm^2 V^{-1} s^{-1} for **BDT(ThBTTh)$_2$**, while 2.4 × 10^{-4} cm^2 V^{-1} s^{-1} for **BDT(BTTh$_2$)$_2$** (Table 2). The former is almost three-order higher than the latter. Since OFETs with neat film samples can not reflect the real charge transportation for the OSC devices, the hole mobility in the blend films composed of the checked compound and $PC_{61}BM$ in 1/1 (w/w) ratio, same to the active layer of the optimized OSC devices, was measured by a space charge-limited current method (SCLC) with a hole-only structure configuration of ITO/PEDOT:PSS/blend film/Au under various film thicknesses (Fig. S6, ESI†). By this means, **BDT(ThBTTh)$_2$**-based blend film gave a hole mobility of 4.7 × 10^{-4} cm^2 V^{-1} s^{-1} in a thickness of 110 nm, while 2.2 × 10^{-4} cm^2 V^{-1} s^{-1} for 95 nm thickness (Table 2). In comparison, the hole mobilities of **BDT(BTTh$_2$)$_2$**–based blend films were 0.69 × 10^{-4} and 0.86 × 10^{-4} cm^2 V^{-1} s^{-1} under the film thicknesses of 100 and 70 nm, respectively. These results again indicate that the former possess larger hole mobility than the latter. Therefore, it is no doubt that the higher charge mobility observed for **BDT(ThBTTh)$_2$** either in neat or blend film is one key factor for its higher OSC performance.

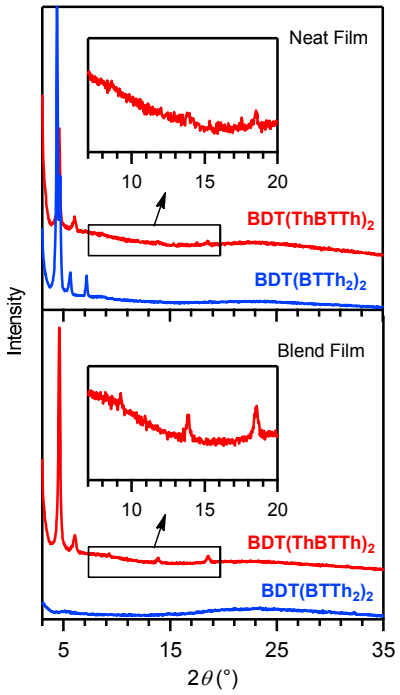

Fig. 5 XRD patterns of **BDT(ThBTTh)$_2$** and **BDT(BTTh$_2$)$_2$** in neat films and blend films with $PC_{61}BM$ (1:1, w/w).

Besides charge mobility, the film structure and morphology also have great influences in device performance. In the X-ray

diffraction (XRD) experiments, the **BDT(ThBTTh)$_2$** pristine film displayed two sharp diffraction peaks at 4.6 and 6.1 °, together with a couple of weak ones around 8.6, 13.8, and 18.5 ° (Fig. 5). The *d*-spacings for these peaks except 6.1 ° are 1.92, 1.02, 0.64, and 0.48 nm, respectively, assignable to 001, 002, 003 and 004 diffraction from a lamellar structure. The d-spacing for the diffraction peak of 6.1 ° is 1.46 nm, which is half of its molecular length (ca. 3.0 nm estimated by DFT geometry optimization). This may suggest the molecules of **BDT(ThBTTh)$_2$** possibly adopt a half-interdigitated configuration along the molecular length direction. In comparison, the pristine film of **BDT(BTTh$_2$)$_2$** also showed sharp diffraction peaks at 4.4, 4.7, 5.6 and 7.2 ° with *d*-spacings of 2.01, 1.89, 1.56 and 1.23 nm, respectively. Since no higher diffraction peak was observed, the assignment of these peaks and the structure of **BDT(BTTh$_2$)$_2$** neat film are not clear at present. These observations clearly indicate both **BDT(ThBTTh)$_2$** and **BDT(BTTh$_2$)$_2$** pristine films have an ordered crystalline structure but with different lattice parameters. However, the situation changed a lot when they were blended with $PC_{61}BM$ (1:1, w/w). In the case of **BDT(ThBTTh)$_2$** blend film, the same series diffraction peaks at 4.6, 6.1, 9.2, 13.9 and 18.5 ° were still observed. This suggests that **BDT(ThBTTh)$_2$** kept the same crystalline structure even in the presence of $PC_{61}BM$. In sharp contrast, no clear XRD peak was observed for the blend film composed of **BDT(BTTh$_2$)$_2$** and $PC_{61}BM$. This result indicates that **BDT(BTTh$_2$)$_2$** changed to amorphous structure, possibly owing to the interference from $PC_{61}BM$.

Atomic force microscopy (AFM) revealed a microphase separation morphology for both blend films (Fig. 6). The domain size was estimated to tens to hundreds nm for the **BDT(ThBTTh)$_2$**-based blend film, while several hundred nm for that based on **BDT(BTTh$_2$)$_2$**. Although both are not ideal, the observed domain size suggests the former is more favourable for OSC applications than the latter. The root-mean-square (RMS) roughness was measured to be 2.3 nm for **BDT(ThBTTh)$_2$** blend film while 2.0 nm for **BDT(BTTh$_2$)$_2$** blend film. These roughness data are comparable and suggest it would not be an important factor for their performance differences. It was reported that certain solvent additive, such as 1,8-diiodoctane (DIO) and polydimethylsiloxane (PDMS), has improved the active layer morphology and thus enhanced cell efficiency for either polymer- or small molecule-based OSCs.[1, 2, 5] Therefore, we checked both DIO and PDMS as solvent additives with various concentrations, but found no improvements in our cases (Table S1, ESI†).

Conclusions

In this study, we have revealed how large impact on its basic properties and photovoltaic performance by changing moiety sequence in chemical structure of a small molecular photovoltaic material. As compared with isomer **BDT(BTTh$_2$)$_2$**, **BDT(ThBTTh)$_2$** having a slightly structural variation in exchange of BT and thiophene positions displays a lower melting point, a blue-shifted absorption spectrum in solution, and a slightly low-lying HOMO. More importantly, **BDT(ThBTTh)$_2$** exhibits a much ordered crystalline structure, especially in the blend film with $PC_{61}BM$, and possesses a much larger hole mobility. All these factors work together, awarding **BDT(ThBTTh)$_2$** a much better OSC performance. Through this study, one may understand the importance of moiety sequence to material photovoltaic performance. Moreover, the so large performance difference between two isomers proves a valid design strategy for high performance optoelectronic materials.

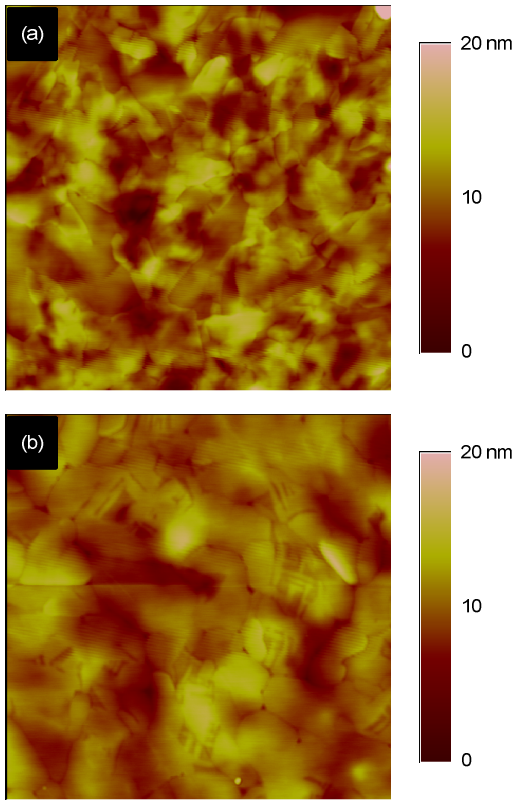

Fig. 6 AFM height images (2 × 2 μm^2) of the blend films of (a) **BDT(ThBTTh)$_2$** and (b) **BDT(BTTh$_2$)$_2$** with $PC_{61}BM$ (1:1, w/w).

Experimental section

Measurements and characterizations

Unless indicated, all commercial reagents were used as received without any further purification. Reaction solvents were dehydrated following standard methods and freshly distilled prior to use. Tetrahydrofuran (THF) and toluene were distilled from a mixture of Na and benzophenone under argon. Compound 2-(5-hexylthiophen-2-yl)-4,4,5,5-tetramethyl-1,3,2-dioxaborolane,[13] 4,7-dibromobenzo[*c*][1,2,5] thiadiazole,14 5-hexyl-2,2'-bithiophene,[15] and 4,8-bis(2-ethylhexoxyl)benzo[1,2-*b*:4,5-*b*']dithiophene-2,6-diyl) bistrimethylstannane[16] were synthesized according to the reported procedures. ^{1}H NMR and ^{13}C NMR spectra were recorded on a Varian Mercury spectrometer operated at 400 MHz and 100 MHz respectively,

using $CDCl_3$ or $C_2D_2Cl_4$ as a solvent and tetramethyl silane as an internal reference. Electron ionization (EI) mass spectra were tested on an Agilent 5973N Mass Spectrometer by an electron impact ionization procedure (70 eV). Matrix-assisted laser desorption/ionization time-of-flight (MALDI-TOF) mass spectroscopy was carried out on a Shimadzu Biotech Axima Performance Mass Spectrometer using dithranol or α-cyano-4-hydroxycinnamic acid as a matrix. UV-vis absorption spectroscopy was performed on a Hitachi U-3310 spectrophotometer. Cyclic voltammetry (CV) was carried out on a CHI 660C electrochemical workstation with a glassy carbon working electrode, a platinum wire counter electrode and a $Ag/AgNO_3$ reference electrode. The samples were casted from chlorobenzene solutions on glassy carbon to form a film then measured in CH_3CN solution containing 0.1 M Bu_4NPF_6 supporting electrolyte at a scan rate of 50 mV s^{-1}. Thermogravimetric analysis (TGA) was carried out on a Q500 TGA instrument under a N_2 flow at a heating rate of 10 °C min^{-1}. Differential scanning calorimetry (DSC) measurements were tested on a Q200 DSC instrument under a N_2 flow at a heating and cooling rate of 10 °C min^{-1}. X-ray diffraction (XRD) was carried out on a PANalytical X'Pert Pro diffractometer using Cu *K*α beam (40 kV, 40 mA) in θ−2θ scans (0.033 Å and 30 s per step). Atomic force microscopy (AFM) was performed on a Veeco Nanoscope IIIa multimode apparatus by a tapping mode with a silicon tip.

Synthesis

4-Bromo-7-(5-hexylthiophen-2-yl)-benzo[*c*][1,2,5]thiadiazole (compound **1**): To a mixture of 2-(5-hexylthiophen-2-yl)-4,4,5,5-tetramethyl-1,3,2-dioxaborolane (529.2 mg, 1.8 mmol), 4,7-dibromobenzo[*c*][1,2,5]thiadiazole (785.7 mg, 2.7 mmol), K_2CO_3 aqueous solution (2.0 M, 9.0 mL) and THF (36 mL), $Pd(PPh_3)_4$ (103.8 mg, 0.09 mmol) was added under Ar. After thoroughly degas by three cycles of freeze-pump-thaw, the reaction mixture was refluxed for 24 h under Ar. Then, cold water was added and the resulted mixture was extracted with dichloromethane several times. The combined organic phase was washed with water, dehydrated over anhydrous $MgSO_4$, and concentrated under a reduced pressure. The residue was subjected to silica gel column chromatography using hexane as an eluent, affording 480 mg compound **1** as yellow solid in a yield of 70%. ^{1}H NMR (400 MHz, $CDCl_3$, δ): 7.88 (d, J = 2.8 Hz, 1H), 7.76 (d, J = 7.6 Hz, 1H), 7.57 (d, J = 7.6 Hz, 1H), 6.84 (d, J = 2.8 Hz, 1H), 2.86 (t, J = 7.2 Hz, 2H), 1.73 (br, 2H), 1.20–1.50 (br, 6H), 0.90 (br, 3H). ^{13}C NMR (100 MHz, $CDCl_3$, δ): 153.79, 151.77, 148.56, 135.87, 132.31, 128.23, 127.43, 125.42, 125.04, 111.55, 31.67, 31.63, 30.38, 28.93, 22.69, 14.20; EI MS m/z: 380 (M^+). HRMS (EI, m/z): $[M+H]^+$ calcd. for $C_{10}H_{17}N_2S_2Br$, 380.0017; found, 380.0022.

4-(5-Hexylthiophen-2-yl)-7-(thiophen-2-yl)-benzo[*c*][1,2,5]thiadiazole (compound **2**): To a mixture of compound **1** (760 mg, 2.0 mmol), thiophen-2-yl boronic acid (1.28 g, 10.0 mmol), K_2CO_3 aqueous solution (2 M, 15.0 mL), and THF (45 mL), $Pd(PPh_3)_4$ (115.4 mg, 0.1 mmol) was added under Ar. After thoroughly degas by three cycles of freeze-pump-thaw, the reaction mixture was refluxed for 24 h under Ar. Then, cold water was added and the resulted mixture was extracted with CH_2Cl_2 several times. The combined organic phase was washed with water, dehydrated over anhydrous $MgSO_4$, and concentrated under a reduced pressure. The residue was subjected to silica gel column chromatography using hexane as an eluent, affording 600 mg compound **2** as yellow solid in a yield of 83%. ^{1}H NMR (400 MHz, $CDCl_3$, δ): 8.09 (d, J = 3.2 Hz, 1H), 7.94 (d, J = 3.2 Hz, 1H), 7.83 (d, J = 7.6 Hz, 1H), 7.77 (d, J = 7.6 Hz, 1H), 7.44 (d, J = 5.2 Hz, 1H), 7.20 (t, J = 4.0 Hz, 1H), 6.87 (d, J = 2.8 Hz, 1H), 2.88 (t, J = 7.6 Hz, 2H), 1.75 (m, 2H), 1.20–1.50 (br, 6H), 0.9 (t, J = 7.2 Hz, 3H). ^{13}C NMR (100 MHz, $CDCl_3$, δ): 152.74, 152.64, 148.11, 139.59, 136.79, 128.06, 127.69, 127.37, 126.65, 126.44, 125.98, 125.41, 125.35, 125.07, 31.72, 31.72, 30.44, 28.98, 22.72, 14.23. EI MS m/z: 384 (M^+). HRMS (EI, m/z): $[M+H]^+$ calcd. for $C_{20}H_{20}N_2S_2$, 384.0789; found, 384.0788.

4-(5-Bromothiophen-2-yl)-7-(5-hexylthiophen-2-yl)-benzo[*c*][1,2,5]thiadiazole (compound **3**): *N*-bromosuccinimide (NBS, 239.1 mg, 1.35 mmol) was slowly added into a solution of compound **2** (508.5 mg, 1.32 mmol) in THF (25 mL). The reaction mixture was stirred overnight shielding from light. Afterwards, the solvent was removed under a reduced pressure. The residue was subjected to silica gel column chromatography using hexane as an eluent, affording 540 mg compound **3** as yellow solid in a yield of 88%. ^{1}H NMR (400 MHz, $CDCl_3$, δ): 7.95 (d, J = 3.6 Hz, 1H), 7.76–7.79 (m, 3H), 7.15 (d, J = 3.6 Hz, 1H), 6.88 (d, J = 3.6 Hz, 1H), 2.88 (t, J = 7.6 Hz, 2H), 1.75 (m, 2H), 1.2–1.5 (br, 6H), 0.9 (t, J = 7.2 Hz, 3H). ^{13}C NMR (100 MHz, $CDCl_3$, δ): 152.44, 152.34, 148.35, 140.92, 136.62, 130.69, 127.91, 126.90, 126.71, 125.40, 125.27, 124.82, 124.31, 114.31, 31.73, 31.70, 30.45, 29.00, 22.74, 14.24. EIMS m/z: 464 (M^+). HRMS (EI, m/z): $[M+H]^+$ calcd. for $C_{20}H_{19}N_2S_3Br$, 461.9894; found, 461.9896.

BDT(ThBTTh)$_2$: A mixture of compound **3** (231 mg, 0.5 mmol), 4,8-bis(2-ethylhexoxyl)benzo[1,2-*b*:4,5-*b*']dithiophene-2,6-diyl) bistrimethylstannane (154.8 mg, 0.2 mmol), $Pd(PPh_3)_4$ (23 mg, 0.02 mmol) and toluene (20 mL) was subjected to degas by three cycles of freeze-pump-thaw and then heated to reflux for 24 h. Then, cold water was added and the resulted mixture was extracted with $CHCl_3$ several times, dried over anhydrous $MgSO_4$, and concentrated under a reduced pressure. The residue was subjected to silica gel column chromatography using hexane and then $CHCl_3$ as an eluent. The crude product was recrystallized in chlorobenzene, affording 140 mg compound **BDT(ThBTTh)$_2$** as dark purple solid in a yield of 58%. ^{1}H NMR (400 MHz, CD_2Cl_4, 110 °C, δ): 7.98 (d, J = 2.0 Hz, 2H), 7.90 (d, J = 2.0 Hz, 2H), 7.76 (d, J = 5.2 Hz, 2H), 7.70 (d, J = 5.2 Hz, 2H), 7.53 (s, 2H), 7.31 (d, J = 2.0 Hz, 2H), 6.79 (d, J = 2.0 Hz, 2H), 4.19 (d, J = 2.8 Hz, 4H), 2.81 (t, J = 4.8 Hz, 4H), 1.82 (m, 2H), 1.19–1.74 (br, 32H), 1.02 (t, J = 4.8 Hz, 6H), 0.93 (t, J = 4.8 Hz, 6H), 0.84 (t, J = 4.8 Hz, 6H). LRMS (MALDI) m/z: 1210.2 (M^+). HRMS (MALDI, m/z): $[M+H]^+$ calcd. for $C_{66}H_{74}N_4O_2S_8$, 1210.3577; found, 1210.3539.

2-(5'-Hexyl-(2,2'-bithiophen)-5-yl)-4,4,5,5-tetramethyl-1,3,2-dioxaborolane (compound **4**): BuLi (5.28 mmol, 1.6 M) was dropwise added into a THF solution (20 mL) of 5-hexyl-2,2'-bithiophene (1.2 g, 4.8 mmol) at -78 °C. Then, the reaction mixture was warmed slowly to 0 °C and kept for 10 min. After cooled down to -78 °C again, the reaction mixture was added with isopropoxyboronic acid pinacol ester (1.16 g, 6.24 mmol). Afterwards, the dry ice bath was removed and the reaction mixture was allowed to warm to room temperature naturally. After water (10 mL) was added to quench the reaction, the resulted mixture was extracted with CH_2Cl_2 several times. The combined organic phase was washed with water, dehydrated over anhydrous $MgSO_4$, and concentrated under a reduced pressure. The residue was subjected to silica gel column chromatography using hexane/CH_2Cl_2 as an eleunt, affording 1.0 g compound **4** as light yellow oil in a yield of 56%. ^{1}H NMR (400 MHz, $CDCl_3$, δ): 7.49 (d, J = 4.8 Hz, 1H), 7.16 (d, J = 4.8 Hz, 1H), 7.04 (d, J = 4.8 Hz, 1H), 6.68 (d, J = 4.8 Hz, 1H), 2.78 (t, J = 10.0 Hz, 2H), 1.67 (b, 2H), 1.20–1.50 (br, 18H), 0.89 (br, 3H).

4-Bromo-7-(5'-hexyl-(2,2'-bithiophen)-5-yl)-benzo[*c*][1,2,5]thiadiazole (compound **5**): A mixture of compound **4** (1.18 g, 3.1 mmol), 4,7-dibromobenzo[*c*][1,2,5]thiadiazole (1.19 g, 4.0 mmol) and a solution of K_2CO_3 (2 M, 22.5 mL), and THF (68 mL) was added with $Pd(PPh_3)_4$ (346 mg, 0.3 mmol) under Ar. After thoroughly degas by three cycles of freeze-pump-thaw, the reaction mixture was refluxed for 24 h under Ar. Then, cold water was added and the resulted mixture was extracted with $CHCl_3$ for several times. The combined organic phase was washed with water, dehydrated over anhydrous $MgSO_4$, and concentrated under in a reduced pressure. The residue was subjected to silica gel column chromatography using hexane/CH_2Cl_2 as an eluent, affording 700 mg compound **5** as yellow solid in a yield of 48%. ^{1}H NMR (400 MHz, $CDCl_3$, δ): 8.09 (d, J = 4.0 Hz, 1H), 7.83 (d, J = 8.0 Hz, 1H), 7.67 (d, J = 8.0 Hz, 1H), 7.17 (d, J = 4.0 Hz, 1H), 7.10 (d, J = 4.0 Hz, 1H), 6.72 (d, J = 4.0 Hz, 1H), 2.81 (t, J = 7.6 Hz, 2H), 1.70 (m, 2H), 1.20–1.50 (br, 6H), 0.9 (t, J = 7.2 Hz, 3H). ^{13}C NMR (100 MHz, $CDCl_3$, δ): 153.76, 151.61, 146.29, 139.89, 136.33, 134.30, 132.25, 128.86, 126.85, 125.03, 124.99, 123.94, 123.79, 111.90, 31.56, 31.56，30.23, 28.77, 22.58, 14.11. LRMS (MALDI) m/z: 461.8 (M^+).

BDT(BTTh$_2$)$_2$: A mixture of compound **5** (231 mg, 0.5 mmol), 4,8-bis(2-ethylhexoxyl)benzo[1,2-*b*:4,5-*b*']dithiophene-2,6-diyl) bistrimethylstannane (154.8 mg, 0.2 mmol), $Pd(PPh_3)_4$ (11.5 mg, 0.01 mmol) and toluene (6.0 mL) was subjected to degas by three cycles of freeze-pump-thaw and heated to reflux for 24 h under Ar. After cold water was added, the resulted mixture was extracted with $CHCl_3$ for several times. The combined organic phase was dried over anhydrous $MgSO_4$ and concentrated under a reduced pressure. The residue was subjected to silica gel column chromatography using hexane and then $CHCl_3$ as an eluent. The separated crude product was recrystallized in $CHCl_3$, affording 120 mg pure **BDT(BTTh$_2$)$_2$** as dark purple solid in a yield of 91%. ^{1}H NMR (400 MHz, CD_2Cl_4, 110 °C, δ): 8.75 (br, 2H), 8.05 (br, 2H), 7.91 (br, 2H), 7.86 (br, 2H), 7.18 (br, 2H), 7.10 (br, 2H), 6.73 (br, 2H), 4.38 (d, J = 2.8 Hz, 4H), 2.83 (d, J = 5.2 Hz, 4H), 1.20–2.0 (br, 34H), 1.15 (t, J = 4.8 Hz, 6H), 1.01 (t, J = 4.8 Hz, 6H), 0.93 (t, J = 4.8 Hz, 6H). LRMS (EI) m/z: 1210 (M^+). HRMS (EI, m/z): $[M+H]^+$ calcd. for $C_{20}H_{20}N_2S_2$, 1210.3577; found, 1210.3559.

Device fabrication and characterization

OSC device fabrication and characterization: The solar cell devices were fabricated with a structure of ITO/PEDOT:PSS/active layer/Ca/Al. A thin layer of PEDOT:PSS (Heraeus Clevios P VP. Al 4083) was spin-coated on top of cleaned ITO glass at 6000 rpm and baked at 140 °C for 15 min, affording a thickness of 23 nm. Then, the substrates were transferred into a N_2-filled glove box. The active layer was spin-coated from warm chlorobenzene solutions containing the checked compounds and $PC_{61}BM$ (Lumitec LT-8905). The thermal anneal at desired temperature for 10 min if applied. Finally, a layer of Ca (10 nm) and a layer of Al (100 nm) were subsequently deposited in the vacuum of 10^{-5} mbar. The active area of all devices is 7 mm^2. Layer thickness was measured on a Veeco Dektak 150 profilometer. Current density-voltage (J-V) curves were recorded with a Keithley 2420 source meter. Photocurrent was acquired upon irradiation using an AAA solar simulator (Oriel 94043A, 450 W) with AM 1.5G filter. The light intensity was adjusted to be 100 mW cm^{-2} using a NREL-certified standard silicon cell (Orial reference cell 91150). External quantum efficiency (EQE) was detected with a 75 W Xe lamp, an Oriel monochromator (74125), an optical chopper, a lock-in amplifier, and a NREL-calibrated crystalline silicon cell.

SCLC device fabrication and characterization: The hole mobility for the blend films of the checked compounds with $PC_{61}BM$ in a weight ratio of 1:1 was measured using hole-only devices with a configuration of ITO/PEDOT:PSS/active layer/Au. The devices were fabricated following the same methods and conditions used for OSCs, except the final metal layer. In these devices, a layer of Au (100 nm) deposited in the vacuum of 10^{-5} mbar was applied as the top electrode. According to the Mott-Gurney law, the SCLC theory can be described as

$$J = \frac{9}{8}\varepsilon_0\varepsilon_r\mu_h\frac{(V_a - V_{bi})^2}{d^3}$$

where J is the current density, ε_0 is the permittivity of free space, ε_r is the relative permittivity of the material, μ_h is the hole mobility, d is the thickness of active layer, V_a is the applied voltage and V_{bi} is built-in voltage.[17]

OFET device fabrication and characterization: For OFET devices, the doped Si wafer with a SiO_2 layer of 300 nm and a capacitance of 11nF cm^{-2} was used as the gate electrode and dielectric layer. Thin films were deposited on octadecyltrichlorosilane (OTS)-treated SiO_2/Si substrates by spin-coating the solutions of **BDT(ThBTTh)$_2$** (10 mg mL^{-1} in chlorobenzene) and **BDT(BTTh$_2$)$_2$** (10 mg mL^{-1} in $CHCl_3$).

Then, gold source and drain contacts (50 nm in thickness) were deposited by vacuum evaporation on top of the active layer through a shadow mask, affording a bottom-gate top-contact device configuration. The ratio between channel length (L) and width (W) was 8.95. Electrical measurements of OFET devices were carried out at room temperature in air using a Keithley 4200 semiconductor parameter analyzer. The field-effect mobility was calculated in the saturation regime by using the equation $I_{DS}= (\mu WC_i/2L)(V_G–V_T)^2$, where I_{DS} is the drain-source current, μ is the field-effect mobility, W is the channel width, L is the channel length, C_i is the capacitance per unit area of the gate dielectric layer, V_G is the gate voltage, and V_T is the threshold voltage.

Acknowledgements

This work was supported by National Natural Science Foundation of China (Nos. 20974119, 90922019, and 21074147), Science and Technology Commission of Shanghai Municipality (No. 13JC1407000), and Chinese Academy of Sciences. We thank Professor Hongxiang Li, Professor Xike Gao, Dr. Xiaolan Qiao and Ms. Zhongli Wang for their help in the OFET measurements.

Notes and references

[a] Laboratory of Synthetic and Self-assembly Chemistry for Organic Functional Molecules, Shanghai Institute of Organic Chemistry, Chinese Academy of Sciences, 345 Lingling road, Shanghai 200032, China.
[b] Department of Chemistry, Zhejiang Sci-Tech University, Hangzhou 310018, China.
[c] Department of Polymer Science and Engineering, Zhejiang University, Hangzhou 310027, China.

† Electronic Supplementary Information (ESI) available: detailed files of TGA, DSC, CV, OFET, SCLC, OSC See DOI: 10.1039/b000000x/

1 (a) L. Dou, J. You, Z. Hong, Z. Xu, G. Li, R. A. Street and Y. Yang, *Adv. Mater.*, 2013, **25**, 6642; (b) A. J. Heeger, *Adv. Mater.*, 2014, **26**, 10.

2 (a) S. Gunes, H. Neugebauer and N. S. Sariciftci, *Chem. Rev.*, 2007, **107**, 1324; (b) J. Chen and Y. Cao, *Acc. Chem. Res.*, 2009, **42**, 1709; (c) Y.-J. Cheng, S.-H. Yang and C.-S. Hsu, *Chem. Rev.*, 2009, **109**, 5868; (d) H. J. Son, F. He, B. Carsten and L. Yu, *J. Mater. Chem.*, 2011, **21**, 18934; (e) H. Ye, W. Li and W. Li, *Chin. J. Org. Chem.*, 2012, **32**, 266; (f) H. Zhou, L. Yang and W. You, *Macromolecules*, 2012, **45**, 607; (g) T. Umeyama and H.Imahori, *J. Mater. Chem. A*, 2014, DOI: 10.1039/c3ta15387h.

3 (a) Z. He, C. Zhong, S. Su, M. Xu, H. Wu and Y. Cao, *Nat. Photonics*, 2012**,** **6***,* 591; (b) C. Cabanetos, A. E. Labban, J. A. Bartelt, J. D. Douglas, W. R. Mateker, J. M. J. Fréchet, M. D. McGehee and P. M. Beaujuge, *J. Am. Chem. Soc.*, 2013**,** **135***,* 4656; (c) I. Osaka, T. Kakara, N. Takemura, T. Koganezawa and K. Takimiya, *J. Am. Chem. Soc.*, 2013, **135**, 8834; (d) N. Wang, Z. Chen, W. Wei and Z. Jiang, *J. Am. Chem. Soc.*, 2013**,** **135***,* 17060; (e) S.-H. Liao, H.-J. Jhuo, Y.-S. Cheng, S.-A. Chen, *Adv. Mater.*, 2013, **25**, 4766; (f) M. Zhang, Y. Gu, X. Guo, F. Liu, S. Zhang, L. Huo, T. P. Russell and J. Hou, *Adv. Mater.*, 2013, **25**, 4944; (g) K. H. Hendriks, G. H. L. Heintges, V. S. Gevaerts, M. M. Wienk and R. A. J. Janssen, *Angew. Chem. Int. Ed.*, 2013, **52**, 8341.

4 J. You, L. Dou, K. Yoshimura, T. Kato, K. Ohya, T. Moriarty, K. Emery, C.-C. Chen, J. Cao, G. Li and Y. Yang, *Nat. Commun.*, 2013, **4**, 1446.

5 (a) A. Mishra and P. Bäuerle, *Angew. Chem. Int. Ed.*, 2012, **51**, 2020; (b) Y. Lin, Y. Li and X. Zhan, *Chem. Soc. Rev.*, 2012, **41**, 4245; (c) Y. Chen, X. Wan and G. Long, *Acc. Chem. Res.*, 2013, **46**, 2645; (d) J. E. Coughlin, Z. B. Henson, G. C. Welch and G. C. Bazan, *Acc. Chem. Res.*, 2014, **47**, 257.

6 Z. Li, G. He, X. Wan, Y. Liu, J. Zhou, G. Long, Y. Zuo, M. Zhang and Y. Chen, *Adv. Energy Mater.*, 2012, **2**, 74; (b) J. Zhou, X. Wan, Y. Liu, Y. Zuo, Z. Li, G. He, G. Long, W. Ni, C. Li, X. Su and Y. Chen, *J. Am. Chem. Soc.*, 2012, **134**, 16345; (c) J. Zhou, Y. Zuo, X. Wan, G. Long, Q. Zhang, W. Ni, Y. Liu, Z. Li, G. He, C. Li, B. Kan, M. Li and Y. Chen, *J. Am. Chem. Soc.*, 2013, **135**, 8484.

7 (a) Y. Sun, G. C.Welch,W. L. Leong, C. J. Takacs, G. C. Bazan and A. J. Heeger, *Nat. Mater.*, 2012, **11**, 44; (b) C. J. Takacs, Y. Sun, G. C .Welch, L. A. Perez, X. Liu, W. Wen, G. C. Bazan and A. J. Heeger, *J. Am. Chem. Soc.*, 2012, **134**, 16597; (c) X. Liu, Y. Sun, L. A. Perez, W. Wen, M. F. Toney, A. J. Heeger and G. C. Bazan, *J. Am. Chem. Soc.*, 2012, **134**, 20609.

8 (a) T. S. van der Poll, J. A. Love, T.-Q. Nguyen and G. C. Bazan, *Adv. Mater.*, 2012, **24**, 3646; (b) V. Gupta, A. K. K. Kyaw, D. H. Wang, S. Chand, G. C. Bazan and A. J. Heeger, *Sci. Rep.*, 2013, **3**, 1965.

9 (a) Y. Li, Y. Cao, J. Gao, D. Wang, G. Yu and A. J. Heeger, *Synth. Met.*, 1999, **99**, 243; (b) J. Zhang, W. Cai, F. Huang, E. Wang, C. Zhong, S. Liu, M, Wang, C. Duan, T. Yang and Y. Cao, *Macromolecules*, 2011, **44**, 894.

10 (a) P. Hohenberg and W. Kohn, *Phys. Rev.*, 1964, **136**, B864; (b) W. Kohn and L. J. Sham, *Phys. Rev.*, 1965, **140**, A1133; (c) C. Lee, W. Yang and R. G. Parr, *Phys. Rev.*, 1988, **B37**, 785; (d) A. D. Becke, *J. Chem. Phys.*, 1993, **98**, 5648.

11 M. J. Frisch, G. W. Trucks, H. B. Schlegel, G. E. Scuseria, M. A. Robb, J. R. Cheeseman, J. A. J. Montgomery, T. Vreven, K. N. Kudin, J. C. Burant, J. M. Millam, S. S. Iyengar, J. Tomasi, V. Barone, B. Mennucci, M. Cossi, G. Scalmani, N. Rega, G. A. Petersson, H. Nakatsuji, M. Hada, M. Ehara, K. Toyota, R. Fukuda, J. Hasegawa, M. Ishida, T. Nakajima, Y. Honda, O. Kitao, H. Nakai, M. Klene, X. Li, J. E. Knox, H. P. Hratchian, J. B. Cross, V. Bakken, C. Adamo, J. Jaramillo, R. Gomperts, R. E. Stratmann, O. Yazyev, A. J. Austin, R. Cammi, C. Pomelli, J. W. Ochterski, P. Y. Ayala, K. Morokuma, G. A. Voth, P. Salvador, J. J. Dannenberg, V. G. Zakrzewski, S. Dapprich, A. D. Daniels, M. C. Strain, O. Farkas, D. K. Malick, A. D. Rabuck, K. Raghavachari, J. B. Foresman, J. V. Ortiz, Q. Cui, A. G. Baboul, S. Clifford, J. Cioslowski, B. B. Stefanov, G. Liu, A. Liashenko, P. Piskorz, I. Komaromi, R. L. Martin, D. J. Fox, T. Keith, M. A. Al-Laham, C. Y. Peng, A. Nanayakkara, M. Challacombe, P. M. W. Gill, B. Johnson, W. Chen, M. W. Wong, C. Gonzalez and J. A. Pople, *Gaussian 03*, Gaussian, Inc., Wallingford CT, 2004**.**

12 (a) J. Nelson, J. J. Kwiatkowski, J. Kirkpatrick and J. M. Frost, *Acc. Chem. Res.*, 2009, **42**, 1768; (b) M. O'Neill and S. M. Kelly, *Adv.*

Mater., 2011, **23**, 566; (c) S. D. Dimitrov and J. R. Durrant, *Chem. Mater.*, 2014, **26**, 616.

13 K.-L. Wu, C.-H. Li, Y. Chi, J. N. Clifford, L. Cabau, E. Palomares, Y.-M. Cheng, H.-A. Pan and P.-T. Chou, *J. Am. Chem. Soc*., 2012, **134**, 7488.

14 J.-T. Wang, H.-Y. Ye, H.-J. Li, C.-Y. Mei, J. Ling, W.-S. Li and Z. Shen, *Chin. J. Chem.*, 2013, **31**, 1367.

15 B. Shaik, J. H. Park, T. K. An, Y. R. Noh, S. B. Yoon, C. E. Park, Y. J. Yoon, Y.-H. Kim and S.-G. Lee, *Tetrahedron*, 2013, **69**, 8191.

16 C.-Y. Mei, L. Liang, F.-G. Zhao, J.-T. Wang, L.-F. Yu, Y.-X. Li and W.-S. Li, *Macromolecules*, 2013, **46**, 7920.

17 (a) C. Goh, R. J. Kline, M. D. McGeheea, E. N. Kadnikova and J. M. J. Fréchet, *Appl. Phys. Lett*., 2005, **86**, 122110; (b) G. Zhao, Y. He, Z. Xu, J. Hou, M. Zhang, J. Min, H.-Y. Chen, M. Ye, Z. Hong, Y. Yang and Y. Li, *Adv. Funct. Mater.*, 2010, **20**, 1480.

Table of Contents

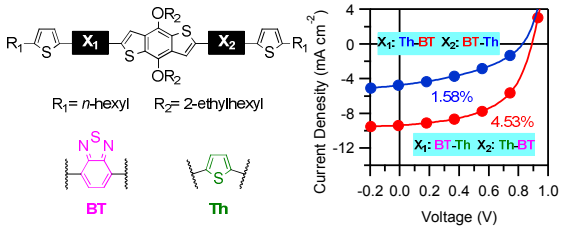

Two isomeric molecules with a structural variation by simply exchanging benzothiadiazole and thiophene positions displayed much different charge transport and photovoltaic performances.